J. Fluid Mech. (1993), *vol.* 251, *pp.* 563–579

The vaporization of a liquid front moving through a hot porous rock

By ANDREW W. WOODS AND SHAUN D. FITZGERALD

Institute of Theoretical Geophysics, Department of Applied Mathematics and Theoretical Physics and Department of Earth Sciences, University of Cambridge, Silver Street, Cambridge CB3 9EW, UK

(Received 30 April 1992 and in revised form 23 December 1992)

We develop an analytical model to describe the generation of vapour as water moves through a hot porous rock, as occurs in hot, geothermal reservoirs. Typically the isotherms in the liquid lag behind the water–vapour interface and so water is supplied to the interface at the interface temperature. This temperature is lower than that in the rock far ahead of the interface. Therefore, as the hot porous rock is invaded with water, it cools and the heat released is used to vaporize some of the water. At low injection rates, vapour formed from the injected liquid may readily move ahead of the advancing liquid–vapour interface and so the interfacial pressure remains close to that in the far field ahead of the interface. The mass fraction that vaporizes is then limited by the superheat of the rock. For larger injection rates, the interfacial vapour pressure becomes considerably greater than that in the far field in order to drive the vapour ahead of the moving interface. As a result, the interfacial temperature increases. The associated reduction in the thermal energy available for vaporization results in a decrease in the mass fraction of vapour produced.

Since the vapour is compressible, the motion of the vapour ahead of the interface is governed by a nonlinear diffusion equation. Therefore, the geometry of injection has an important effect upon the mass fraction of water that vaporizes. We show that with a constant supply of water from (i) a point source, the mass fraction of water which vaporizes increases towards the maximum permitted by the superheat of the rock; (ii) a line source, a similarity solution exists in which the mass fraction vaporizing is constant; and (iii) a planar source, the liquid–vapour interface steadily translates through the rock with a very small fraction of the injected water vaporizing.

1. Introduction

Geothermal reservoirs are typically located near regions of volcanic or tectonic activity, and lie at depths of up to several kilometres below the Earth's surface; they consist of hot, fractured rock and sediment whose interstices are saturated with fluid (Elder 1981; Wohletz & Heiken 1992). The hottest geothermal reservoirs may have temperatures as high as 200–300 °C. In such reservoirs, the fluid is typically in the vapour phase with pressures in the range 1–30 atmospheres (Elder 1981; Pruess *et al.* 1987). Interest in such reservoirs stems from their potential to generate power by drawing off the vapour along wells in order to drive turbines (DiPippo 1980). Power plants have been installed at several reservoirs, including the Geysers reservoir in California and the Lardarello field in Italy (Elder 1981; Grant, Donaldson & Bixley 1982). As vapour is extracted from such reservoirs, the mass of vapour and hence pressure in the reservoir decreases (Enedy 1989); this causes a reduction in the rate of

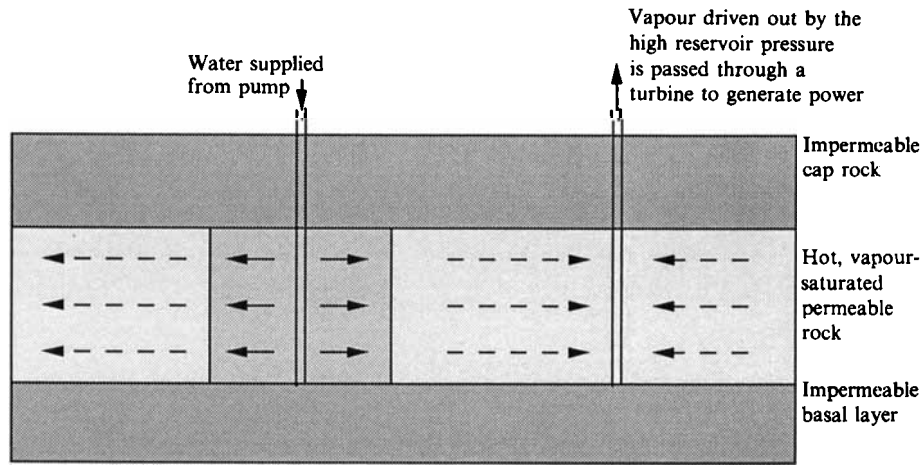

FIGURE 1. Schematic of a geothermal reservoir, bounded between two layers of impermeable rock. Water injected into the left-hand well bore advances into the rock, with vapour forming at the leading edge. This vapour may subsequently be extracted from the extraction well on the right-hand side.

extraction of vapour and hence power production. However, this vapour can be regenerated: if the reservoir temperature increases with depth sufficiently rapidly then a gravitationally stable layer of liquid may form above the high-pressure vapour region (Schubert & Straus 1980). In such a situation, as the vapour pressure decreases, the liquid–vapour interface descends into the reservoir. This causes some vaporization and a concomitant increase in the vapour pressure. However, natural recharge of vapour is usually insufficient to maintain the reservoir pressure (Kerr 1991). Therefore, at several geothermal reservoirs, cold water is actively injected into the reservoir through well bores (figure 1) (Elder 1981; Pruess *et al.* 1987). As this injected liquid moves into the hot rock, a fraction of the liquid vaporizes.

The mechanism by which relatively cold liquid vaporizes as it invades a hot, permeable rock is therefore an important and fundamental process, of interest for both the natural and forced recharge of geothermal reservoirs: the purpose of this paper is to expose the underlying physical processes which control such vaporization. In particular, we investigate how the heat transfer between the hot rock and the water is coupled to the dynamics by which the newly formed vapour can migrate ahead of the liquid–vapour interface. We use this model to determine how the vaporization process depends upon the rate of supply of water, the geometry of the source of water and the intrinsic properties of the reservoir.

In the first part of the paper, we analyse the heat transfer as cold water migrates through a hot rock and establish conditions under which the effects of thermal diffusion may be neglected; following Bodvarsson (1972) we show that in a porous rock the isotherm speed is smaller than the interstitial liquid velocity because the fluid only migrates through the pores whereas the heat must migrate through both the pores and the solid matrix. We extend this result to show that even if some of the liquid vaporizes, the isotherms still lag behind the liquid–vapour interface; we deduce that the liquid is supplied to the vaporizing interface at the interface temperature.

In the second part of the paper, we use these results to derive a new model of a moving vaporization front invading a hot porous rock. Pruess *et al.* (1987) presented a simpler linearized model of such a front and derived a quasi-linear similarity solution describing the growth of a circular front in a porous layer. Using this solution, they recognized that as the flow rate increases, the rate of vapour production decreases. We

generalize the analysis to investigate the role of the geometry and rate of injection upon the production of vapour. We present a family of nonlinear similarity solutions describing the vaporization which ensues when water is injected at suitable rates from point, line and planar sources. We also present some numerical calculations which describe the time-dependent generation of vapour and motion of the liquid–vapour interface resulting from the steady injection of water from a point, line or planar source. We compare these numerical solutions with some asymptotic solutions, which are valid at long times. We conclude with a brief discussion of the implications of our results in the context of geothermal reservoirs.

2. Advection and diffusion of isotherms in a hot permeable rock

We consider the migration of water through a hot permeable rock of uniform porosity ϕ ($\phi \ll 1$) and permeability k. In this section we consider the isothermal host rock to be saturated with water, so that there is no phase change at the leading edge of the injected water (figure 2*a*). We generalize this analysis in §3, where we consider the host rock to be vapour saturated (figure 2*b*). In the water-saturated region, the conservation of mass may be simply expressed as

$$\phi \frac{\partial \rho_w}{\partial t} + \nabla \cdot (\boldsymbol{u} \rho_w) = 0, \tag{1}$$

where ρ_w is the density of the water and $\boldsymbol{u}$ is the Darcy velocity, defined as the volume flux per unit area of rock. The water actually migrates through the rock with an interstitial velocity $\boldsymbol{u}/\phi$.

If the water percolates through the rock sufficiently slowly then the rock and the fluid are in local thermodynamic equilibrium. As a result, the conservation of energy is most easily expressed in terms of the change in enthalpy, $\overline{\rho C_p}\theta$, associated with a given control volume due to the net heat transfer, by both advection and diffusion, through the surfaces of the control volume

$$\frac{\partial(\overline{\rho C_p}\theta)}{\partial t} + \nabla \cdot (\boldsymbol{u} \rho_w C_{pw} \theta = \nabla \cdot (\bar{K} \nabla \theta), \tag{2}$$

where C_{pw} and C_{pr} are the specific heats of the water and rock,

$$\overline{\rho C_p} = \phi \rho_w C_{pw} + (1-\phi) \rho_r C_{pr}, \tag{3}$$

K_w and K_r are the thermal conductivities of the water and rock and we adopt the approximation

$$\bar{K} = \phi K_w + (1-\phi) K_r, \tag{4}$$

for the mean conductivity (Batchelor 1974; Dullien 1992). Ignoring variations in the specific heat C_{pw} with temperature, we may combine (1) and (2) to obtain an equation describing the evolution of the temperature field in the rock

$$\overline{\rho C_p} \frac{\partial \theta}{\partial t} + \rho_w C_{pw} \boldsymbol{u} \cdot \nabla \theta = \nabla \cdot (\bar{K} \nabla \theta). \tag{5}$$

In the absence of diffusion, the ratio, λ, of the velocity of surfaces of constant temperature u_θ to the actual velocity of the fluid (u/ϕ) is given by

$$\lambda = \left(\frac{u_\theta}{u/\phi} \right) = \frac{\phi \rho_w C_{pw}}{\rho C_p}. \tag{6a, b}$$

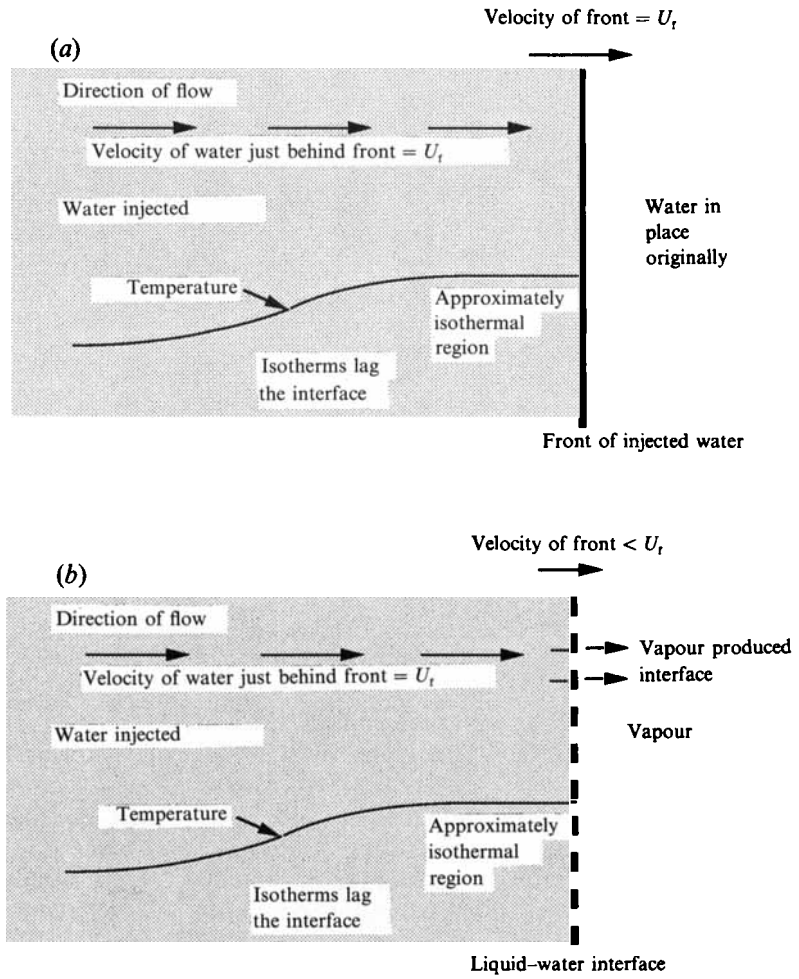

FIGURE 2. Schematic showing the migration of isotherms through a permeable rock as it is invaded with water in the case of (*a*) no vaporization, and (*b*) vaporization from an advancing interface.

Since $\lambda < 1$, the rate of migration of the isotherms is smaller than that of fluid parcels, which propagate at a rate u/ϕ. We deduce that if thermal diffusion is unimportant, then the water just behind the leading front of injected water will have the same temperature as the front (Bodvarsson 1972). Essentially, the fluid loses memory of its initial temperature since it travels faster than the isotherms and so is heated up by the surrounding rock (figure 2*a*).

2.1. *Effects of thermal diffusion*

We may ignore the effects of thermal diffusion at the leading edge of the new liquid, $r(t)$, if the advective heat flux far exceeds the diffusive heat flux,

$$\lambda \dot{r} r/\kappa\phi \gg 1, \tag{7}$$

where $\kappa = \bar{K}/\overline{\rho C_p}$. Suppose the water is supplied from a symmetric source in n dimensions, such that the volume flow rate (per unit area or length for one- or two-dimensional sources) is $(\beta+1)A_n t^{\beta}$. Then, the leading edge of the newly input liquid, $r(t)$, is given by

$$r(t) = \left(\frac{nA_n}{S_n} t^{(\beta+1)}\right)^{1/n}, \tag{8}$$

where $S_n = 1, 2\pi$ or 4π for one-, two- or three-dimensional sources ($n = 1, 2$ or 3). Substituting this expression for $r(t)$ into (7) gives an expression for the conditions under which thermal diffusion is negligible:

$$\lambda \frac{\beta+1}{n} \left(\frac{n^2 A_n^2}{S_n^2} t^{2(\beta+1)-n} \right)^{1/n} \gg \kappa\phi. \tag{9}$$

There are three different situations in which condition (9) holds; these depend upon the rate of injection (β) and the geometry of injection (n).

First, if $2(\beta+1) > n$, then (9) holds in the long-time limit

$$t \gg \tau, \tag{10a}$$

where

$$\tau = \left(\frac{n\phi\kappa S_n^{2/n}}{\lambda(\beta+1) n^{2/n} A_n^{2/n}} \right)^{n/(2(\beta+1)-n}. \tag{10b}$$

Thus, after a sufficiently long time the effects of thermal diffusion become unimportant. This case includes the steady injection of water from a planar source ($n = 1$). For example, with typical steady injection rates $10^{-5} \leqslant A_1 \leqslant 10^{-4}$ m/s, thermal diffusion plays no role in determining the interfacial temperature after a time $t \sim 1$–10^2 s, and the fluid is supplied to the interface at the interfacial temperature (equation (6)).

In the second situation, $2(\beta+1) = n$, the rate of advance of the injected fluid front is directly proportional to the rate of diffusion of the isotherms. In this case the effects of thermal diffusion are only important in a region of size $d_\kappa \sim (\kappa t)^{\frac{1}{2}}$ near the source, while the interface is located a distance $d_f \sim (nA_n)^{1/n} t^{\frac{1}{2}}$ from the source. Therefore, $d_f \gg d_\kappa$ if

$$\frac{\lambda(\beta+1)}{\phi n} \left(\frac{nA_2}{S_n} \right)^{2/n} \gg \kappa, \tag{11}$$

in which case the rate of diffusion of isotherms is much smaller than the rate of advance of the interface and thermal diffusion plays no role in determining the interface temperature. For example, in typical, steady two-dimensional injection ($n = 2$) into a geothermal reservoir, $10^{-4} \leqslant A_2 \leqslant 10^{-3}$ m^2/s. Therefore $d_\kappa \sim (10^{-2}$–$10^{-1})\, d_f$ and thermal diffusion is indeed negligible.

In the third situation, $2(\beta+1) < n$, condition (9) only holds in the short-time limit $t \ll \tau$. For typical steady injection from a point source ($n = 3$), $10^{-3} \leqslant A_3 \leqslant 10^{-2}$ m^3/s and so $\tau \sim 10^{17}$–10^{19} s. This is beyond the typical timescale of interest for a geothermal reservoir and again it is valid to neglect diffusion.

3. The fluid–vapour interface

When the host rock is vapour saturated rather than liquid saturated, and the input fluid is relatively cold, some of the liquid supplied to the advancing liquid–vapour interface vaporizes. Therefore, the interface moves less rapidly than the liquid because of mass transfer across the interface (figure 2*b*). We must therefore show that the interface still propagates faster than the isotherms, so that the fluid arrives at the interface at the interface temperature. For simplicity, in order to elucidate some of the fundamental controls upon the rate of phase change we assume that the interface remains planar (Pruess *et al.* 1987).

Let us denote the rate of advance of the fluid interface as uR/ϕ where $R < 1$. We deduce that a fraction $1-R$ of the fluid which is supplied to the interface actually vaporizes. Owing to the thermal inertia of the rock (§2) this vapour migrating ahead

of the liquid–vapour interface heats up to the far-field temperature of the rock, T_∞ say, irrespective of the interfacial temperature. Let us suppose that liquid of temperature T_f is supplied to the interface, of temperature T_i, where $T_f \leqslant T_i$. Then, in steady state, as the rock is invaded with fluid, the heat released by the rock as it cools from the far-field temperature to that at the interface is used to heat the liquid to the interface temperature, to vaporize a fraction $1-R$ of this liquid and then to heat up this new vapour to the temperature of the far field:

$$\phi\rho_w(T_i - T_f) + \phi(1-R)\rho_w(h_{v\infty} - C_{pw}T_i) = R(1-\phi)\rho_r C_{pr}(T_\infty - T_i). \tag{12a}$$

Here $h_{v\infty}$ denotes the enthalpy of the vapour in the far field, C_p denotes the specific heat and ρ the density.

We can rearrange the Stefan condition (12a) to show that

$$R = \frac{\phi\rho_w(T_i - T_f) + \phi\rho_w(h_{v\infty} - C_{pw}T_i)}{\phi\rho_w(h_{v\infty} - C_{pw}T_i) + (1-\phi)\rho_r C_{pr}(T_\infty - T_i)}. \tag{12b}$$

Combining equations (3), (6b) and (12b) it follows that $R > \lambda$ because $h_{v\infty}$ includes the latent heat of vaporization and therefore exceeds $C_{pw}T_\infty$ so that

$$(h_{v\infty} - C_{pw}T_i) > C_{pw}(T_\infty - T_i). \tag{13}$$

We deduce that the liquid–vapour interface migrates faster than the isotherms. Therefore, as in §2, in the absence of thermal diffusion, the fluid will be supplied to the liquid–vapour interface with the interface temperature, $T_f = T_i$, and the Stefan condition (12) becomes

$$\phi(1-R)\rho_w(h_{v\infty} - C_{pw}T_i) = R(1-\phi)\rho_r C_{pr}(T_\infty - T_i). \tag{14}$$

As a result, the initial temperature at which the fluid is input into the rock has no effect upon the rate of vaporization.

3.1. *Effects of thermal diffusion*

As in §2, there are three distinct situations in which thermal diffusion may be neglected, depending upon the rate and geometry of injection. Although in each situation the mass fraction of the input liquid that vaporises, $1-R$, may change with time, in §6, we show that it asymptotes to a constant value. However, in geothermal systems, even during the transient stage, $R > 0.1$ (§4), and so by assuming that the system has asymptoted to this constant value, we can estimate the times for which thermal diffusion is unimportant.

In the first case, $2(\beta+1) > n$, the lengthscale of the liquid-filled region becomes $r(t) = ((nA_n/S_n)Rt^{(\beta+1)})^{1/n}$ and so thermal diffusion ceases to be important for times

$$t \gg \tau R^{-2/(2(\beta+1)-n)}, \tag{15}$$

where τ is defined in (10b). In the next section, we show that under typical conditions in geothermal systems, $R \geqslant 0.1$, and so condition (15) is typically satisfied for $t \gg O(10^2$–10^4 s) for steady injection from a planar source.

In the second case, $2(\beta+1) = n$, the condition that thermal diffusion does not affect the interfacial temperature becomes

$$\frac{\lambda(\beta+1)}{n}\left(\frac{nA_n R}{S_n}\right)^{2/n} \gg \kappa\phi. \tag{16}$$

For steady injection from a line source ($n = 2$) with typical injection rates $A_2 \sim 10^{-4}$–10^{-3} m^2/s condition (16) holds.

In the third case, $2(\beta+1) < n$, effects due to thermal diffusion may only be neglected for times

$$t \ll \tau R^{-2/(2(\beta+1)-n)}. \tag{17}$$

Again adopting the typical rates of injection used in §2, for injection at a steady rate from a point source thermal diffusion is negligible for $t \ll 10^{15}$–10^{17} s.

3.2. *The Clausius–Clapeyron relation*

We assume that the fluid and vapour are in thermodynamic equilibrium at the liquid–vapour interface and neglect any effects of surface tension. Thus the interfacial pressure and temperature are related by the Clausius–Clapeyron equation, which has the empirical form

$$T_{\rm sat}(P) = 6.7P^{0.23} \tag{18}$$

(Haywood 1972) in the temperature range $150 < T < 240$ °C, where T and P represent the temperature and pressure in SI units. By combining (14) and (18) we may calculate the flux of vapour produced at the interface as a function of the interfacial pressure. We now present a model describing the motion of the vapour ahead of the interface; this provides a second relationship between the interfacial pressure and the vapour flux migrating ahead of the interface, thereby completing the mathematical model of this phase-change interface.

4. The vapour region

Darcy's law

$$\mu \boldsymbol{v} = -k\nabla P \tag{19}$$

describes the velocity $\boldsymbol{v}$ of the vapour as a function of the applied pressure gradient ∇P when the interstitial Reynolds number is small (Dagan 1989; Pruess *et al.* 1987; Dullien 1992). Here μ represents the dynamic viscosity of the vapour and k the permeability. For vapour flow through porous rocks, the pore Reynolds number $Re = \rho u d/\mu \sim u$ for a typical pore size of $d \sim 10^{-5}$ m; in this case, our theory is valid for vapour which migrates at a rate $u \leqslant 0.1$ m/s. The conservation of mass within the vapour region is given by

$$\phi \frac{\partial \rho_{\rm v}}{\partial t} + \nabla(\boldsymbol{v}\rho_{\rm v}) = 0, \tag{20}$$

where $\rho_{\rm v}$ is the vapour density. Finally, the equation of state relates the density $\rho_{\rm v}$, temperature θ and pressure P of the vapour:

$$P = \rho_{\rm v} R_{\rm g} \theta, \tag{21}$$

where $R_{\rm g}$ is the gas constant for vapour (Young 1988).

We may combine (19)–(21) to obtain the nonlinear equation

$$\left(\frac{P}{\theta}\right)_t - \frac{k}{\phi\mu}\nabla\cdot\left(\frac{P}{\theta}(\nabla P)\right) = 0. \tag{22}$$

According to this equation, the similarity lengthscale L over which changes occur in time t is given by $L \sim ((kP/\phi\mu)\,t)^{\frac{1}{2}}$. In geothermal systems, this is typically much larger than the similarity lengthscale of thermal diffusion $(\kappa t)^{\frac{1}{2}}$, where κ is the thermal diffusion coefficient, since $((kP/\phi\mu)(1/\kappa))^{\frac{1}{2}} \sim 10^2$. Therefore, the temperature field within the vapour region adjusts to the far-field vapour temperature through thermal conduction across a very narrow thermal boundary layer near the interface;

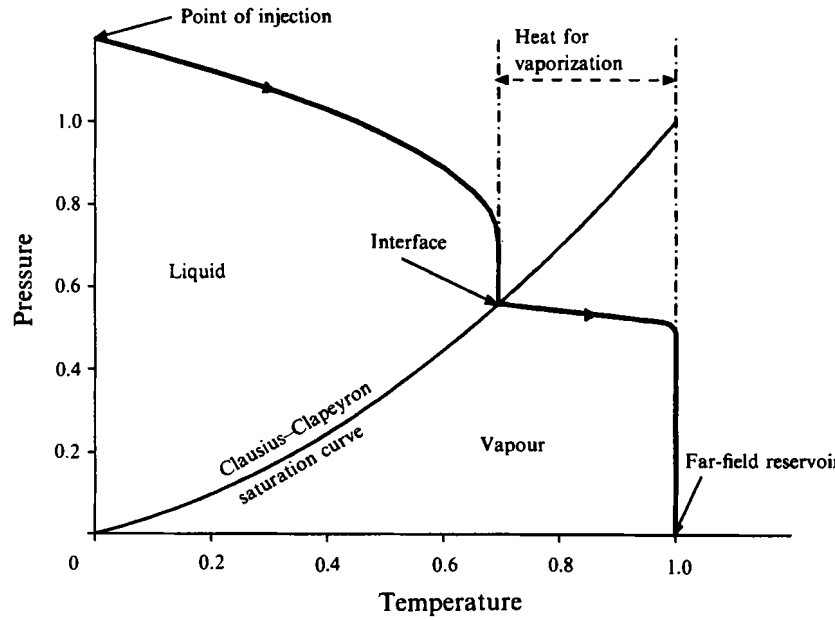

FIGURE 3. Schematic of the vaporization front, showing the temperatures ahead of and behind the interface. Thick solid line shows the path followed by fluid from the point of injection to the far field of the reservoir.

furthermore, according to (22), the pressure remains nearly constant across this boundary layer (figure 3). Beyond this narrow boundary layer, the vapour attains the far-field temperature and so the pressure distribution ahead of the interface is governed by the isothermal equation

$$\frac{\partial P}{\partial t} - \frac{k}{\phi\mu}\nabla\cdot(P\nabla P) = 0. \tag{23}$$

Since the thermal boundary layer ahead of the interface is very thin, the change in the heat content of the boundary layer as it expands is several orders of magnitude smaller than the heat transferred through the interface by the vapour; therefore, even in a system evolving with time, to leading order, the conservation of enthalpy across the interface and thermal boundary layer is indeed given by (12*b*).

4.1. *Similarity solutions*

Since the vapour is compressible, it is driven away from the interface diffusively (equation (23)). For convenience we define a reference diffusion coefficient $\alpha = k(P_{\rm sat}(T_\infty) - P_\infty)/\phi\mu$, where $P_{\rm sat}(T)$ is the saturation pressure at temperature T. If vapour is generated at an appropriate rate by the advancing liquid front, then a self-similar vapour distribution develops ahead of the interface, $r = \chi(2\alpha t)^{\frac{1}{2}}$, where the dimensionless similarity variable is $\eta = r/(2\alpha t)^{\frac{1}{2}}$. For injection from an n-dimensional axisymmetric source, such similarity solutions arise if the fluid is injected into the rock at a rate proportional to $t^{n/2-1}$, and if a constant fraction, $1-R$ say, of the water vaporizes. In n-dimensions, equation (23) then simplifies to the dimensionless form

$$-\eta^n p_\eta = [(p_1+p)(\eta^{n-1}p_\eta)]_\eta, \tag{24}$$

where the dimensionless pressure p is defined by the expression

$$P = P_\infty + p(P_{\rm sat}(T_\infty) - P_\infty) \tag{25}$$

and p_1 is the dimensionless background pressure $p_1 = P_\infty/(P_{\rm sat}(T_\infty) - P_\infty)$.

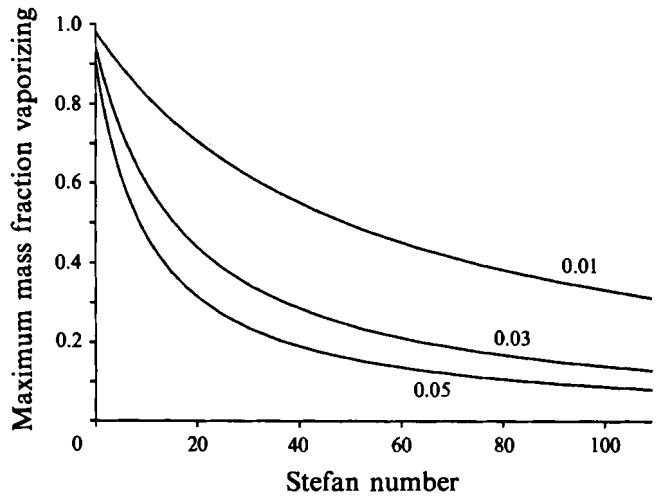

FIGURE 4. The maximum mass fraction vaporized as a function of the reservoir Stefan number for several values of porosity. Typical reservoir Stefan numbers are in the range 10^{-1}–10^{3}.

We solve (24) subject to the constraint of zero motion in the far field,

$$p \to 0 \quad \text{as} \quad \eta \to \infty, \tag{26}$$

and use conservation of mass and enthalpy at the liquid-vapour interface, $\eta = \chi$,

$$(p+p_1)p_\eta = -\left(\frac{\chi(1-R)}{R}\right)\frac{\rho_w R_g T_i}{P_{sat}(T_\infty)-P_\infty} \tag{27}$$

and

$$R = \frac{S+(1-\hat{T})}{S+(1-\hat{T})(1+(1-\phi)\rho_r C_{pr}/\phi\rho_w C_{pw})}, \tag{28}$$

where the Stefan number

$$S = \frac{h_{v\infty}-C_{pw}T_\infty}{C_{pw}(T_\infty - T_{sat}(P_\infty))} \tag{29}$$

represents the ratio of the heat of vaporization at the far-field temperature to the heat required to increase the temperature of the liquid from $T_{sat}(P_\infty)$ to T_∞, and $\hat{T} = (T_i - T_{sat}(P_\infty))/(T_\infty - T_{sat}(P_\infty))$ represents the dimensionless interfacial temperature. We also assume that the interfacial temperature cannot exceed that of the far field. Therefore, $0 < p_i < 1$.

Equation (28) shows that the mass fraction vaporized, $(1-R)$, has an upper bound, $(1-R_u)$, which occurs when the interfacial pressure equals that of the far field, and the rock releases the maximum thermal energy for vaporization (i.e. $p_i = 0$ and $\hat{T} = 0$). Also, the mass fraction vaporized falls to zero when the interfacial temperature equals the saturation temperature associated with the far-field pressure (i.e. $p_i = 1$ and $\hat{T} = 1$). In figure 4, we show how the maximum mass fraction that may be vaporized $(1-R_u)$ varies with Stefan number for three different value of the porosity. Note that for low injection rates, thermal diffusion in the liquid region becomes important (§3) and the problem is more complex.

The interfacial pressure and hence the mass fraction vaporizing are functions of several dimensionless parameters. These include the dimensionless rate of supply of fluid to the interface, χ^2/R (for line source injection), the far-field pressure, p_1, which imposes a lower bound upon the rate of diffusion of vapour away from the interface (equation (24)), and the Stefan number S.

5. A parametric study of injection similarity solutions

We have solved equation (24) subject to the boundary conditions (18), (26) and (28) numerically to determine the dependence of the interfacial pressure and mass fraction vaporizing as a function of the three dimensionless parameters described above. We consider injection from an axisymmetric line source, which admits a similarity solution when the liquid is supplied at a constant rate. This allows us to identify and explain the controls exerted upon the rate of vaporization by these dimensionless parameters.

5.1. *The rate of supply of fluid to the interface,* χ^2/R

As the rate of injection increases, the mass fraction vaporized decreases and the interfacial pressure increases (figure 5*a*, *b*). These results may be readily understood by considering the changes in the interfacial conditions with injection rate. For low injection rates, little vapour is produced, and therefore the interfacial pressure remains small, $p_i \sim 0$. As a result, the mass fraction vaporizing is a maximum since the maximum amount of thermal energy available for vaporization is released from the rock as it is invaded by the liquid and cools. However, as the rate of supply of fluid to the interface increases, the interfacial pressure increases in order to drive the vapour ahead of the moving liquid front (figure 5*b*). As a result, the interfacial temperature increases, (18), and the heat transfer available for vaporization decreases. Therefore, the mass fraction that vaporizes decreases with injection rate. However, the total amount of vapour produced per unit time continues to increase with increasing flow rate (figure 5*c*); the increase in the interfacial pressure simply means that the efficiency of vapour production, defined as the amount of vapour produced per unit mass of liquid injected, is reduced (figure 5*a*).

As the porosity of the host rock increases, the mass fraction vaporized decreases since there is less energy available per unit mass of injected fluid. The main effect is that with a higher porosity, more fluid is present per unit volume.

5.2. *The reservoir pressure*

The effective diffusion coefficient within the vapour region (24) is dependent upon the far-field pressure, p_1, as well as the dynamic pressure within the moving injected vapour, p. The typical range of values for p_1 is $0.1 < p_1 < 0.4$, and by definition p lies in the range 0–1. As the rate of injection increases, the pressure p near the interface increases towards unity from zero and so the local diffusion coefficient close to the interface also increases. At low rates of injection the diffusion coefficient $(p+p_1)$ asymptotes to the background pressure, p_1, since $p_1 > p$. However, at high rates of injection, the local diffusion coefficient close to the interface is dominated by the dynamic pressure p since $p \gg p_1$. This increase in the local diffusion coefficient, especially close to the interface, results in a higher mass fraction vaporizing than would be predicted from a model in which the diffusion coefficient is taken to be the constant p_1 (figure 6, dashed line). Thus, the effect of the increase in the vapour diffusion coefficient with pressure upon the mass fraction vaporizing can be large.

Pruess *et al.* (1987) approximated the diffusion coefficient (p_1+p) by the constant value $\frac{1}{2}(p_1+p_i)$, where p_i is the interfacial pressure. This quasi-linear solution is shown in figure 6 by the dot-dashed line. The approximate diffusion coefficient used by Pruess *et al.* (1987) is smaller than the true value near the interface. However, in the far field it is greater than the true value, and hence the Pruess model leads to the prediction of a greater mass fraction vaporizing.

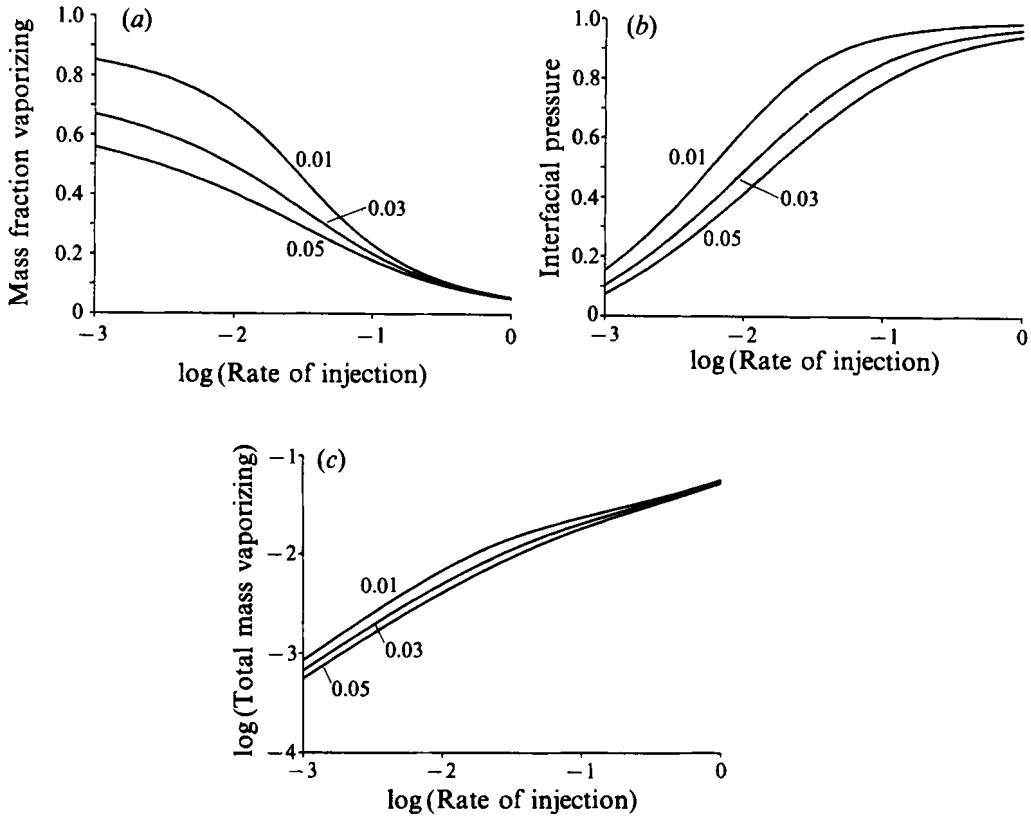

FIGURE 5. Variation of (*a*) the mass fraction vaporized; (*b*) the interfacial pressure and (*c*) the total mass vaporized as a function of the dimensionless rate of supply of fluid to the interface, χ^2/R. Curves are given for three typical values of the rock porosity.

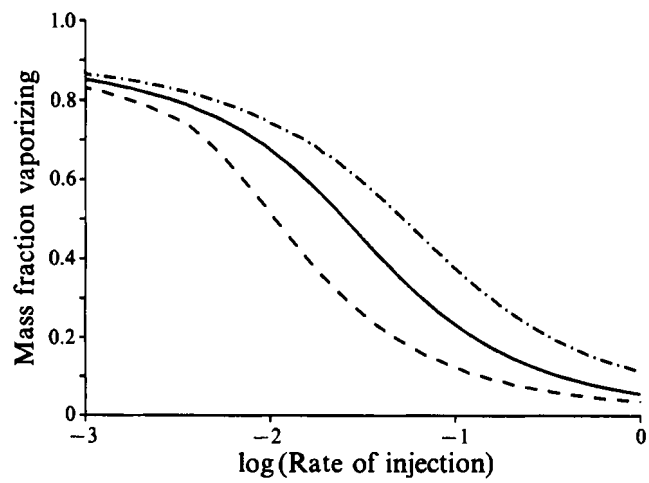

FIGURE 6. Variation of the mass fraction vaporized as a function of the rate of injection, χ/R for rock porosity 0.01. The full nonlinear solution is shown with a solid line, and the solution in which the diffusion coefficient $(p+p_1)$ is replaced by the far-field pressure p_1 is shown with the dashed line. The quasi-linear approximation adopted by Pruess *et al.* is shown as the dot-dashed line.

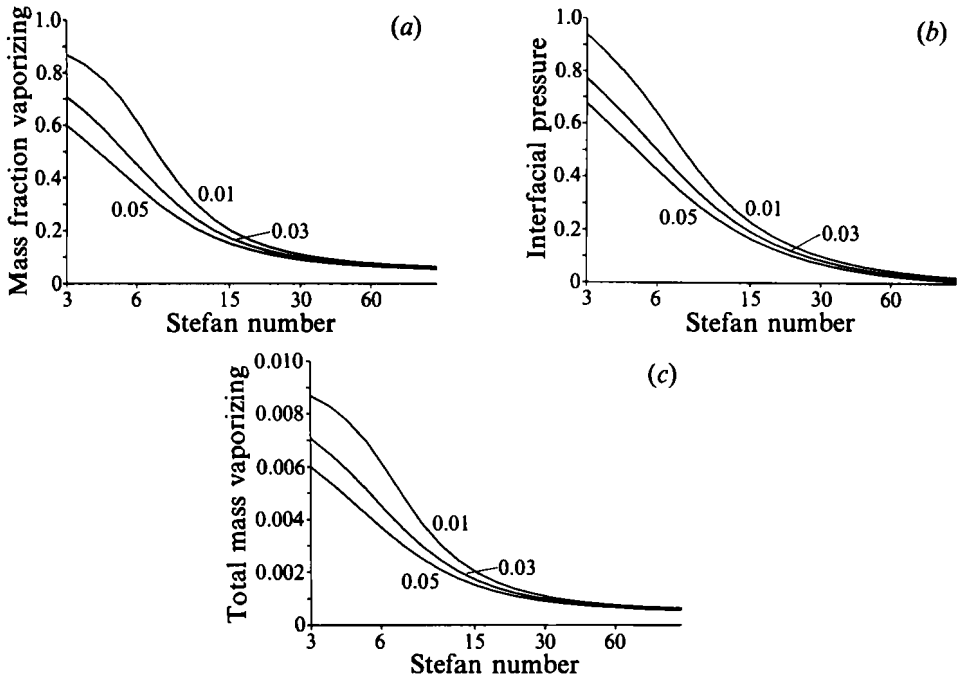

FIGURE 7. (*a*) The mass fraction vaporized, (*b*) the interfacial pressure and (*c*) the total mass vaporized as a function of the reservoir Stefan number. Curves are given for several values of the porosity, and a dimensionless injection rate of 0.01.

5.3. *The Stefan number*

As the superheat, expressed by the parameter S, increases, the heat required for vaporization increases, thereby decreasing the mass fraction vaporized (figure 7*a*) and decreasing the interfacial pressure (figure 7*b*). As a result, the total amount of vapour produced also decreases (figure 7*c*). Note that increasing the Stefan number is equivalent to decreasing the superheat of the rock.

6. Injection at point, line and planar sources

We now consider the effect of injecting fluid from planar or point sources in comparison to that from a line source discussed above. In the similarity solutions, the fluid–vapour interface migrates at a rate $r = 2\chi(\alpha t)^{\frac{1}{2}}$, and so the fluid must be supplied to the interface with velocity $\partial r/\partial t = \chi(\alpha/t)^{\frac{1}{2}}/R$. Hence, for a similarity solution, with axisymmetric injection in n dimensions, the injection rate (per unit length or surface area) is of the form (figure 8*a*)

$$Q(t) = \left(\frac{\chi^2\alpha}{R^2}\right)^{n/2} t^{(n-2)/2}. \tag{30}$$

In figure 8(*b*) we show how the fraction of injected fluid that vaporizes varies as a function of the rate of supply of liquid to the interface per unit area, χ/R, in each of these injection geometries.

6.1. *Planar source*

Equation (30) shows that in one dimension ($n = 1$), a self-similar vaporization front only develops if the flow rate is of the form $Q \sim t^{-\frac{1}{2}}$, essentially since the vapour diffuses ahead of the interface. If the liquid flux does not decay as fast as $t^{-\frac{1}{2}}$, then the new

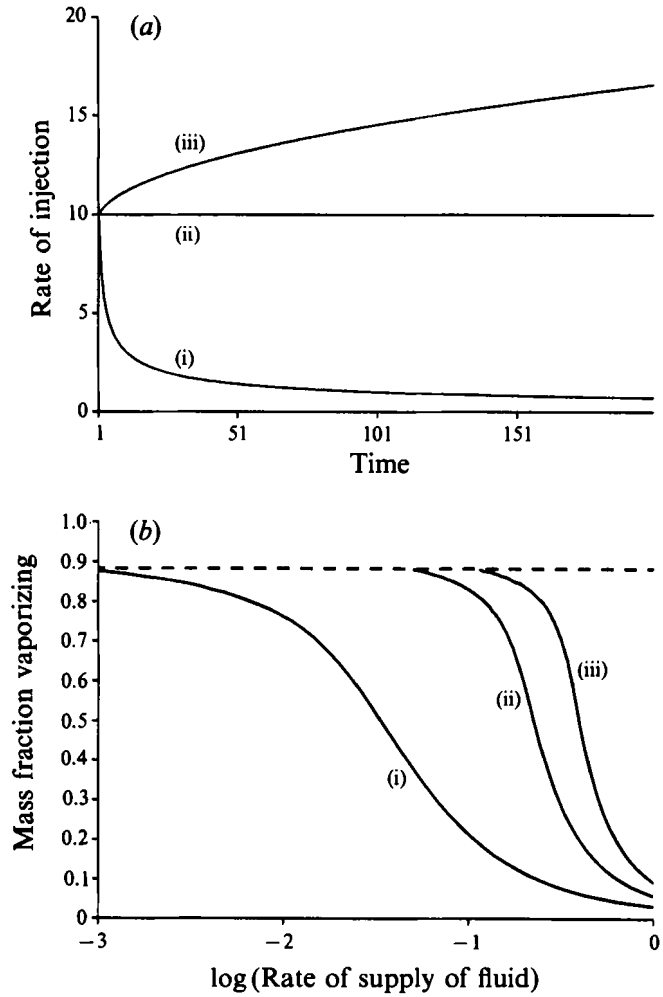

FIGURE 8. (*a*) The rate of injection of mass as a function of time for similarity solutions in one (i), two (ii) and three (iii) dimensions. (*b*) The mass fraction vaporized as a function of the rate of supply of fluid per unit area, χ/R, for injection in one (i), two (ii) and three (iii) dimensions for rock of porosity 0.01. The horizontal dashed line represents the maximum mass fraction that may vaporize.

vapour accumulates ahead of the interface, and the mass fraction of injected water which vaporizes decreases with time until very little of the input fluid actually vaporizes. For example, when the water is input at a constant rate, a steadily translating vaporization front develops in which only a very small fraction of the water vaporizes. For a steady input of water at a rate $Q = (U/R)$ in which the interface advances at a rate U, and a mass fraction $1-R$ vaporizes, equation (23) has solution $P(\xi)$ where $\xi = x - Ut$ and

$$-UP_\xi = \frac{k}{\phi\mu}(PP_\xi)_\xi. \tag{31}$$

In a reservoir of large extent, $P \to P_\infty$ as $\xi \to \infty$ and so

$$-U(P_i - P_\infty) = \frac{k}{\phi\mu}[PP_\xi]_i. \tag{32}$$

Combining this with the equation of conservation of mass across the interface

$$U\left(\frac{1-R}{R}\right)\rho_w = \frac{\rho_v k}{\mu}[P_\xi]_i = \frac{-P_i k}{\mu R_g \theta_\infty}[P_\xi]_i \tag{33}$$

where θ_∞ denotes that the temperature is evaluated in degrees Kelvin, we obtain the relation

$$R = \frac{1}{1-(\phi/R_g\theta_\infty)(P_i - P_\infty)}. \tag{34}$$

Combining this with (12*a*) and (18) we find the difference in temperature across the interface $\Delta T = T_\infty - T_i$ to be

$$\Delta T \sim \left(\frac{\phi^2}{(1-\phi)\rho_r C_{pr}}\right)\left(\frac{1}{R_g\theta_\infty}\right)(P_i - P_\infty)(h_{v\infty} - C_{pw}T_\infty). \tag{35}$$

Our calculations suggest that $1-R \sim 10^{-4}$ in this steady solution.

6.2. *Point source*

In three-dimensional injection, the surface area available for vaporization increases rapidly with radius. In order that the fraction vaporizing remains constant with time, fluid must be injected at an ever increasing rate proportional to $t^{\frac{1}{2}}$, so that the radius of the fluid region grows at a rate $t^{-\frac{1}{2}}$ to keep pace with the vapour, which diffuses ahead of the interface at a rate $t^{-\frac{1}{2}}$. If the rate of input of fluid grows more slowly than $t^{\frac{1}{2}}$ then the fraction vaporizing tends to increase with time; this is because the pressure gradient required to remove the vapour from the interface decreases as the surface area increases, and so the interfacial pressure and hence temperature decrease, thereby releasing more energy for vaporization. In this case, thermal diffusion in the liquid eventually becomes important and the above solution breaks down.

6.3. *Numerical solutions*

In order to illustrate these effects we have solved the full, time-dependent nonlinear diffusion equations, for steady injection in one, two and three dimensions. We used a simple predictor-corrector algorithm (Ames 1977) for this integration, and checked the accuracy of the programme by comparing the numerical results with the similarity solutions.

In figure 9, we present the numerical solution of the time-dependent diffusion equation, for steady injection from point, line and planar sources. Figure 9(*a*) shows the mass fraction vaporized as a function of time; figure 9(*b*) shows the total mass of vapour produced as a function of time; figure 9(*c*) shows the interfacial pressure as a function of time; and figure 9(*d*) shows the radius of the region occupied by the liquid as a function of time.

For injection of water from a point source, the interfacial pressure decreases towards that of the far field, since, as the surface area of the advancing fluid front increases, the vapour requires a much smaller pressure gradient to drive it away from the advancing interface; as a result, the liquid fraction that can vaporize eventually becomes limited by the maximum heat that may be released by the rock as it is invaded by water and cools. After a time of the order $\tau \sim Q^{\frac{2}{3}}/\alpha$, the interfacial pressure asymptotes to the value $p_i \sim 0$, and the mass fraction vaporized attains the maximum value $(1-R_u)$ (figure 3). Beyond this time, the mass fraction that vaporizes is nearly constant, and so the radius of the region occupied by liquid increases as $r \sim Q^{\frac{1}{3}}R_u^{\frac{1}{3}}t^{\frac{1}{3}}$. This may be seen

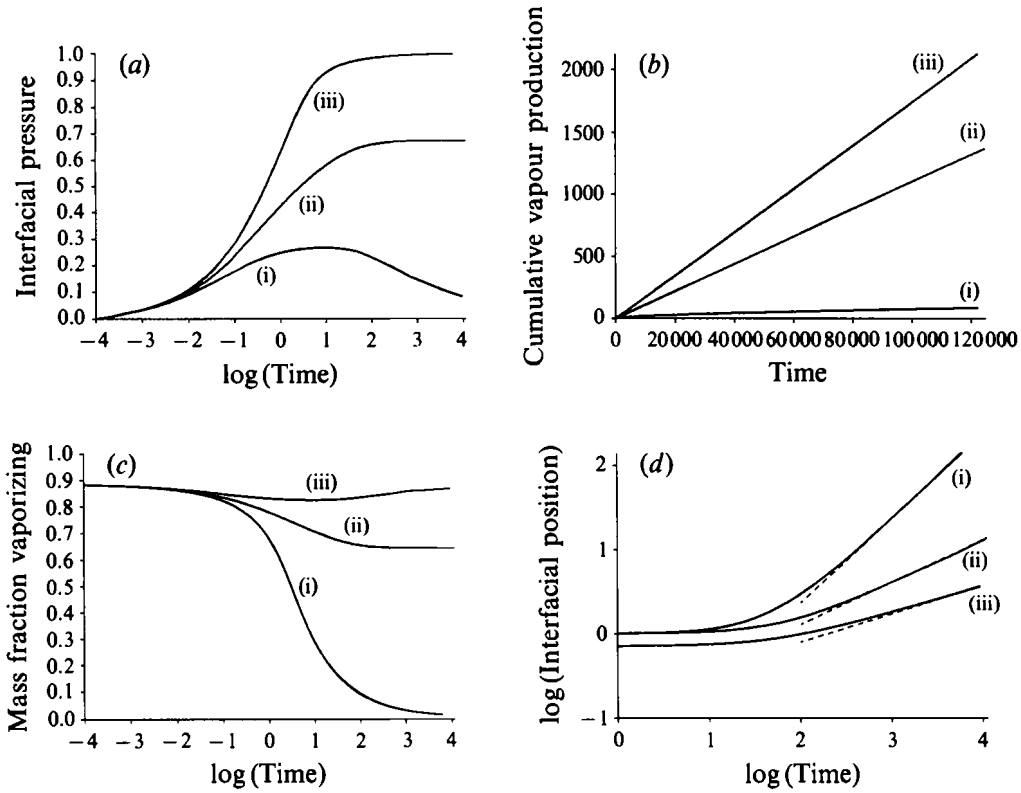

FIGURE 9. Variation of (*a*) the mass fraction vaporized; (*b*) total mass vaporized; (*c*) the interfacial pressure, and (*d*) the radius of the region occupied by liquid as a function of time, for injection at a constant rate in one (i), two (ii) and three (iii) dimensions. The asymptotic scalings $r \sim t, t^{\frac{1}{2}}, t^{\frac{1}{3}}$ are shown as dotted lines. Rock porosity is 0.01 and rate of injection is 0.02. In the two and three dimensional calculations, the initial radius is $r = 1.0$.

in figure 9(*d*) in which the numerical solution converges to the dashed asymptotic line (iii) $r \sim t^{\frac{1}{3}}$. As shown in §3, thermal diffusion in the liquid region eventually becomes important as the interface slows down. The present asymptotic results only hold for times t such that thermal diffusion is unimportant (equation (17)). This requires $t \ll 10^{15}$–10^{17} s which is beyond the time of interest, and so it is valid to ignore such effects.

In figure 9(*d*), we also present a numerical calculation which shows that when liquid is injected in one dimension at a steady rate, the mass fraction steadily decreases because the vapour accumulates ahead of the interface. However, eventually, after a time of the order $\tau \sim Q/\alpha$, a steadily translating vaporization front, (31)–(35), develops.

7. Conclusions

We have presented a new model which describes the generation of vapour following the injection of cold water into a hot rock of large extent. The isotherms in the water region lag behind the fluid front as long as the water is injected sufficiently fast so that thermal diffusion is unimportant. In this case the mass fraction of the injected water that can vaporize is independent of the injection temperature, and instead depends only upon the rate and geometry of injection. Owing to the compressibility of the vapour,

the vapour migrates ahead of the moving fluid front according to a nonlinear diffusion equation, in which the diffusivity increases linearly with the pressure.

We have presented a number of new similarity solutions which describe the generation of vapour when water is supplied at a suitable rate from a point, line or planar source. These solutions show that at low flow rates, the mass fraction of vapour which may be produced from the injected fluid is limited by the thermal energy available in the hot rock, while at high flow rates it is limited by the rate at which the vapour can diffuse ahead of the fluid interface. Indeed, as the flow rate increases, a larger pressure gradient is required in the vapour ahead of the interface, in order that it can escape from the advancing liquid. This increases the interfacial temperature, and thereby reduces the thermal energy available to vaporize the fluid, causing a decrease in the mass fraction that can vaporize. With a larger background pressure, the vapour is able to diffuse ahead of the liquid–vapour interface more rapidly, thereby increasing the mass fraction of vapour produced. As the Stefan number of vaporization increases, the mass fraction vaporized decreases.

Since the vapour diffuses ahead of the liquid–vapour front, the steady injection of water from an axisymmetric line source admits similarity solutions. However, with steady injection of water from a point source, the mass fraction vaporizing increases towards the maximum value given by the superheat of the rock; this is because the liquid–vapour interface advances more slowly than the rate at which vapour diffuses ahead of the interface. Finally, for steady injection from a planar source, vapour accumulates ahead of the liquid–vapour interface, causing a decrease in the mass fraction of liquid that can vaporize, until the system asymptotes towards a steadily translating liquid–vapour front, in which a very small constant fraction of the water vaporizes.

This study has shown that the effect of injecting water into a hot rock at very high flow rates is to fill the rock with relatively hot water while producing a relatively small mass of vapour per unit mass injected. In contrast, by injecting the water at much lower flow rates, a much larger mass of vapour may be produced per unit mass of liquid injected, and the residual water in the reservoir has a much lower temperature. The latter procedure thus results in the extraction of a much greater fraction of the thermal energy stored in the rock.

We are grateful for discussions with John Hinch and for the comments of the referees. S.F. would like to thank the NERC and GeoScience Ltd. for a CASE studentship.

REFERENCES

AMES, W. F. 1977 *Numerical Methods for Partial Differential Equations*. Academic.

BATCHELOR, G. K. 1974 Transport properties of two-phase materials with random structure. *Ann. Rev. Fluid Mech.* **6**, 227–255.

BODVARSSON, G. 1972 Thermal problems in the siting of reinjection wells. *Geothermics* **1**(2), 63–66.

DAGAN, G. 1989 *Flow and Transport in Porous Formations*. Springer.

DIPIPPO, R. 1980 *Geothermal Energy as a Source of Electricity*. Washington DC: US Dept. Energy.

DULLIEN, F. A. L. 1992 *Porous Media – Fluid Transport and Pore Structure*, pp. 1–574. Academic.

ELDER, J. 1981 *Geothermal Systems*. Academic.

ENEDY, K. L. 1989 The role of decline curve at The Geysers. *Geoth. Res. Counc. Trans.* **13**, 383–391.

GRANT, M. A., DONALDSON, I. G. & BIXLEY, P. F. 1982 *Geothermal Reservoir Engineering*. Academic.

HAYWOOD, R. W. 1972 *Thermodynamic Tables in SI (Metric) Units*. Cambridge University Press.

KERR, R. A. 1991 Geothermal tragedy of the commons. *Science* **253**, 134–135.

PRUESS, K., CALORE, C., CELATI, R. & WU, Y. S. 1987 An analytical solution for heat transfer at a boiling front moving through a porous medium. *Intl J. Heat Mass Transfer* **30**, 2595–2602.

SCHUBERT, G. & STRAUS, J. M. 1980 Gravitational stability of water over steam in vapour-dominated geothermal systems. *J. Geophys. Res.* **85**, 6505–6512.

WOHLETZ, K. & HEIKEN, D. 1992 *Volcanology and Geothermal Energy*. University of California Press.

YOUNG, J. B. 1988 An equation of state for steam for turbomachinery and other flow calculations. *J. Engng Gas Turbines Power* **110**, 1–7.